Environmental Science Advances

ROYAL SOCIETY OF CHEMISTRY

PAPER

View Article Online
View Journal | View Issue

Check for updates

Cite this: *Environ. Sci.: Adv.*, 2026, **5**, 853

Investigation of Zn-, Pb-, and Cd-containing nanoparticles in Canadian urban and Arctic environments: a comprehensive study utilizing single particle inductively coupled plasma mass spectrometry for characterization

Richard Macedo de Oliveira, *[ab] Dorthe Dahl-Jensen [ac] and Feiyue Wang [ab]

Measuring metal-containing nanoparticles (NPs) in the environment requires sensitive analytical techniques capable of determining the concentration and elemental composition, particle mass and size. Here we report the characterization of Zn-, Pb-, and Cd-containing NPs by single-particle inductively coupled plasma mass spectrometry (spICP-MS) in snow samples collected from two vastly different sites in Canada: an urban environment from Winnipeg and a remote location at the Müller Ice Cap in Axel Heiberg Island of the Canadian Arctic. Average mass concentrations of Zn-, Pb-, and Cd-containing NPs in fresh snow samples from the urban location ranged from 0.7–149, 1.5–296 and 0.2–1.6 ng L^{-1}, respectively. These concentrations accounted for 0.05–17% of total dissolved (operationally defined as the fraction filtered by a 0.45 μm membrane) concentrations of Zn, 0.2–31.5% of Pb, and 0.05–2.2% of Cd for Cd in the urban snow samples. Mass concentrations for Zn- and Pb-containing NPs in snowpits at depths of 10 to 60 cm from the Müller Ice Cap ranged from 10.0 to 297 ng L^{-1} (or 2.4–28.8% of the total concentration) for Zn and 0.5 to 2.9 ng L^{-1} (or 0.9–4.0% of the total concentration) for Pb. Cd-containing NPs were not detectable in the Müller Ice Cap snowpit. A contrary characteristic in the average equivalent diameter for Zn- and Pb-containing NPs was observed in Winnipeg and Müller Ice Cap snow. The average equivalent diameter of Zn-containing NPs in the urban snow (78.5–116.4 nm) was smaller than that from the High Arctic site, whereas the average equivalent diameter of Pb-NPs in the urban snow was 4.8-fold larger than in the High Arctic snow. Additionally, analysis of Pb isotopic ratios indicated that anthropogenic aerosols in the urban snow predominantly originated from North America, primarily *via* vehicular traffic and various industrial sources. Conversely, aerosols in the Arctic snow were derived from a combination of natural and anthropogenic sources, notably from Asia and North America.

Received 7th August 2025
Accepted 4th February 2026

DOI: 10.1039/d5va00258c

rsc.li/esadvances

Environmental significance

Advances in nanotechnology have increased the presence of metal-containing nanoparticles (NPs) in the environment, raising concerns about their potential effects on ecosystems and human health due to their high reactivity. The release of Zn-, Pb-, and Cd-NPs occurs through natural, incidental, and human activities; however, their fate, concentration, and transport, especially in the Arctic, are poorly understood. Research on atmospheric metallic nanoparticles has been limited due to analytical challenges. In this study, metal-containing NPs were characterized in snow samples from urban and Arctic systems, using single particle inductively coupled plasma mass spectrometry. Results show the presence of Zn-, Pb-, and Cd-containing NPs in urban and Arctic snow and that they primarily originate from traffic emissions and natural or human sources in the Arctic.

1. Introduction

Over the past decades, nanotechnology development has led to an increase in the concentration and diversity of nanoparticles (NPs) in the environment, raising concerns over their potential effects on the ecosystem and human health.[1] One special concern is metal-containing NPs (MNPs), such as metal NPs, metal oxide NPs, or mixed NPs containing metal and organic

[a]*Centre for Earth Observation Science, University of Manitoba, Winnipeg, Manitoba, R3T 2N2, Canada. E-mail: Richard.Oliveira@umanitoba.ca*

[b]*Department of Environment and Geography, University of Manitoba, Winnipeg, Manitoba, R3T 2N2, Canada*

[c]*Niels Bohr Institute, Physics of Ice, Climate and Earth, University of Copenhagen, Copenhagen, Denmark*

Open Access Article. Published on 05 February 2026. Downloaded on 4/22/2026 12:07:22 PM. This article is licensed under a Creative Commons Attribution-NonCommercial 3.0 Unported Licence.

© 2026 The Author(s). Published by the Royal Society of Chemistry

Open Access Article. Published on 05 February 2026. Downloaded on 4/22/2026 12:07:22 PM. This article is licensed under a Creative Commons Attribution-NonCommercial 3.0 Unported Licence.

compounds, which are used in various applications.[2] MNPs have low mass, high chemical reactivity and oxidation capacity, very high surface-to-volume ratio, and carry different surface charges due to their shape, degree of fragmentation, and surface chemical modification.[2] As a result, several MNPs, including Zn, Pb, and Cd, have been connected to adverse effects on humans as they can be readily inhaled from the air through the respiratory system, reaching internal organs including the brain and the bloodstream, increasing the incidence of respiratory and cardiovascular problems, among various health issues.[3,4] Particles with dimensions of 10–100 nm can enter and may be deposited in the bronchioles and alveoli with an efficiency of 20–60%; however, the elimination efficiency of MNPs is not fast as their interaction with cells can be prolonged, causing toxic effects.[4]

The presence of MNPs in the atmosphere can be attributed to natural, anthropogenic and incidental processes.[5] The main contributors are natural sources, such as volcanic eruptions, nucleation in some coastal areas, and mineral, geological, and biological processes.[5] For instance, a volcanic eruption can release several million tons of MNPs into the atmosphere.[5] In addition, dust storms and cosmic dust are significant sources of MNPs. On the other hand, industrial processes, such as metalworking, waste incinerators, and chemical industries, are examples of anthropogenic sources of MNPs in the atmosphere.[2] A major contribution to NPs in the urban air is traffic-related (incidental processes), which could reach concentrations of 10^5–10^8 NPs cm^{-3}.[2] NPs are directly emitted into the air through exhaust processes, *e.g.*, engines, gasoline, diesel, fuel additives, lubricant oils, and catalysts. Non-exhaust traffic sources are related to the tire and brake dust, releasing MNPs, such as Pb, Zn, and Cd, among others, depending on the composition of the brake lubricants, fillers, frictional additives, linings, and tire composition.[2,6] For instance, abraded yellow paint was found to be a significant source of $PbCrO_4$,[7] and road dust was estimated to contribute to 5–55% for resuspended ultrafine particles containing MNPs, including ZnO of various sizes (<100 nm), shapes and compositions.[6,8]

Once released into the atmosphere, NPs are often attached to larger particulate matters (PM) and transported over long distances, including the Arctic,[2] although their presence and dynamics in the Arctic remain poorly known. Two studies in the Canadian Arctic have shown the presence of Ag-, Cu- and Si-NPs in microbial communities in soils at Alexandra Fjord in Nunavut and at Daring Lake in Northwest Territories, although in low concentrations (0.066%).[9,10] In addition to long-distance transport, local industrial activities in the Arctic also emit MNPs, such as from mining and oil and gas extraction.[11] Furthermore, waste burning, biomass burning, and forest fires produce emissions of reactive gases and aerosol particles, which can potentially enhance the concentration of MNPs in the Arctic atmosphere.[11] The occurrence of fine PM and trace gases during winter and early spring, known as Arctic haze, may also contribute to the presence of NPs. During wintertime, cold temperatures and surface-based temperature inversions can trap emitted pollution locally.[11]

Snow provides a valuable medium to evaluate MNPs in the air as it removes or scavenges suspended PMs during wet deposition.[12] MNPs are incorporated into the snow porous structure and accumulated in the snowpack, making it convenient to sample, especially in remote locations such as the Arctic.

Due to their relatively low metal concentrations in environmental samples, generally at ng L^{-1}, matrix complexity and elemental background levels, the measurements of MNPs are often challenging using conventional analytical techniques, including scanning (SEM) or transmission electron microscopy (TEM) with energy-dispersive X-ray analysis (EDX), dynamic light scattering (DLS) and differential centrifugal sedimentation (DSC).[13] In this context, single particle inductively coupled plasma mass spectrometry (spICP-MS) has emerged as a promising and alternative technique for MNP characterization, including Ag-NPs, TiO_2, Au-NPs, and ZnO.[14–19] SpICP-MS is a useful technique for NP measurements due to its capability for particle counting (detecting ion pulses); the measurements are performed on a particle-by-particle basis.[20–22]

This study aims to monitor and characterize Zn-, Pb-, and Cd-containing NPs in snow samples collected from urban (Winnipeg, Canada) and Arctic (Axel Heiberg Island, Canada) sites using spICP-MS.

2. Materials and methods

2.1. Reagents

All the sample preparation and analyses were undertaken in a Class-100 Ultra-Clean Trace Elements Laboratory (UCTEL) at the University of Manitoba (UM). A high-purity water (18.2 MΩ cm; Milli-Q® Advantage A10Millipore Sigma, United States) was used for sample treatment and dilutions. Individual stock solutions of Zn, Pb and Cd of 10 mg L^{-1} from PlasmaCAL (SCP Science, Canada) were used for the analyte quantification in the snow samples. All solutions were diluted to 0.01 to 500 μg L^{-1} in 1% (v/v) freshly distilled HNO_3 (Fisher Chemicals, Canada) for calibration curves and to set response factors for ^{66}Zn, ^{208}Pb, and ^{111}Cd. Two trace-elements-in-water reference materials, TM-27.4 (Environment and Climate Change Canada) and 1643f (National Institute of Standard and Technology, USA), were measured to verify the accuracy of the measurements.

In addition, Au-NPs of 10, 30, and 50 nm (suspended in PEG carboxyl) from Nanocomposix (San Diego, CA, USA) were used as reference materials for evaluating single particle size and transport efficiency. Each Au nanosphere stock solution of 0.05 mg mL^{-1} was diluted to 5.0 ng L^{-1} in ultrapure water and prepared daily for analysis. The Au-NP solutions were sonicated for 5 min in an ultrasonic bath (VWR, USA) prior to analysis to ensure sample homogeneity.

2.2. Snow sampling

The urban snow samples were collected from Winnipeg, Canada (49°53′ N, 97°08′ W) from November 2022 to April 2023. Freshly fallen snow was collected from various locations in the city, six of which were from the downtown area and two from

 © 2026 The Author(s). Published by the Royal Society of Chemistry

Open Access Article. Published on 05 February 2026. Downloaded on 4/22/2026 12:07:22 PM. This article is licensed under a Creative Commons Attribution-NonCommercial 3.0 Unported Licence.

the UM campus, as shown in Fig. S1. The sampling time corresponded to the northern hemisphere winter and spring seasons, and the ambient air temperatures ranged from −1 to −18 °C. The "clean hands/dirty hands" protocol was followed to prevent sample cross-contamination.[23] All samples were stored in new polypropylene Falcon® conical tubes (Corning, USA) and kept at −20 °C until analysis.

The remote snow samples were collected from a snowpit at the Müller Ice Cap on Axel Heiberg Island (79°45′ N, 91°00′ W) in the Canadian Arctic (Fig. S1). The sampling occurred on May 23, 2023, corresponding to the spring season, at an ambient air temperature of −22.5 °C. A snowpit was dug out to a total depth of 60 cm. The exterior wall surface of the snowpit was removed, and snow samples were collected in 500 mL Teflon bottles. The Teflon bottles were precleared in a solution containing 5% (v/v) of phosphate-free detergent (Citranox®, USA) for one week, followed by being rinsed thoroughly with high-purity water. The cleanness of the bottles was confirmed by acceptably low concentrations of trace elements in the residual water (blank levels: 6.0, 0.8, and 0.2 ng L^{-1} for Zn, Pb, and Cd, respectively). A total of six snowpit samples from depths ranging from 10 cm to 60 cm were collected, following the same "clean hands/dirty hands" protocol mentioned above. The samples were transported as melted water and refrozen at −20 °C until analysis.

Twenty-four hours before the measurements, the snow samples were melted at 4 °C, followed by filtration through a 0.45 μm PES (polyethersulfone) syringe filter (Thermo Fisher, USA) to remove larger suspended particulate matter. To ensure thorough homogenization of the suspension particles, the melted samples were sonicated for 5 min in an ultrasonic bath prior to being aspirated to the ICP-MS.

2.3. Instrumentation

2.3.1. spICP-MS analysis and data processing. Single particle characterization was performed on an Agilent 8900 ICP-MS/MS instrument equipped with nickel sampler and skimmer cones, a concentric glass nebulizer, a quartz spray chamber, and a quartz torch containing a 1 mm diameter injector. The instrument was operated in the single-particle mode and tuned daily to optimize sensitivity. The raw data were exported and processed using the SPCal software (version 1.1.11), employing automatic threshold selection with 5-sigma ($\alpha = 2.87 \times 10^{-7}$) criterion for Gaussian filtering and formula C ($\alpha = 0.001$) for Poisson filtering.[24] The operational ICP-MS parameters are summarized in Table S1.

The monitored masses were measured in the Time-Resolved Analysis (TRA) mode, recording the signal intensity for each element consecutively for 60 s using a dwell time of 100 μs. The samples and solutions were aspirated at a flow rate of approximately 0.35 mL min^{-1}. During tandem MS, the helium gas mode was used solely for monitoring ^{66}Zn at a flow rate of 2 mL min^{-1}. The software calculated the transport efficiency to obtain the NP equivalent diameter and elemental compositions. The transport efficiency is determined by the ratio of particles arriving in the plasma to those in the original suspension. For this study, the transport efficiency was calculated to be 3–4%, using a reference nanoparticle solution of 30 nm Au-NPs.

After each run, a washing solution containing 1% (v/v) HCl and 1% (v/v) HNO_3 was introduced to the nebulizer for 1 min to prevent memory effects during the measurements (washout particles that could be sticking in the tubing).

The particle equivalent diameter distribution is a crucial parameter in determining the properties of NPs. In this study, the particle diameter and mass were calculated assuming a spherical particle shape and a specific chemical composition (Zn-NPs, Pb-NPs, and Cd-NPs). The chemical composition/mass fraction and particle density significantly impact the equivalent diameter distribution. This study used particle density values of 7.13, 11.35, and 8.65 g cm^{-3} for Zn, Pb, and Cd, respectively, to determine the particle equivalent diameter distribution.

The limits of detection size (LOD_{size}) corresponded to the automatic thresholds provided by SPCal for Gaussian and Poisson filters, as defined by the equations reported by Lockwood *et al.*[24]

2.3.2. Analyses of the metal concentrations and Pb isotope ratios by ICP-MS/MS. Concentrations of ^{66}Zn, ^{111}Cd, and ^{208}Pb in urban and Arctic snow samples were determined by the conventional ICP-MS (Agilent 8900 ICP-MS/MS). Calibration standards were prepared with concentrations ranging from 0.01 to 500 μg L^{-1}. Additionally, two reference materials (1643f from NIST and TM-27.4 from ECCC) were analyzed to verify measurement accuracy. All solutions were prepared by diluting in freshly doubly distilled 1% (v/v) HNO_3. To evaluate total dissolved concentration, snow meltwater samples were filtered through a 0.45 μm PES filter prior to analysis; therefore, results are reported as total concentrations.

The Pb isotope ratio was determined using the 8900 ICP-MS/MS instrument previously described. The instrument operated in Spectrum mode and was tuned daily to optimize ion sensitivity. Measurements were conducted with no gas mode monitoring ions at m/z values of 204, 206, 207, and 208. Each measurement consisted of 1000 sweeps, with ten replicates analyzed per sample. A dwell time of 0.1 ms was employed for each mass. Consequently, the total acquisition time per sample was approximately 3.25 minutes, encompassing both sample uptake and post-analysis rinsing cycles.

To minimize potential mass bias during the determination of Pb isotope ratios *via* ICP-MS/MS, a bracketing technique using the NIST SRM 981 standard was implemented. The Pb isotope ratios of NIST SRM 981 at 1.0 μg L^{-1} were measured before and after each replicate analysis of the snowpit and surface snow samples.

3. Results

3.1. Zn-, Pb- and Cd-containing NPs in the urban snow

Zn- and Pb-containing NPs were detected in all eight urban snow samples collected from Winnipeg, with varying concentrations and equivalent diameters. Cd-containing NPs were also detected in 37.5% of the samples. The detection thresholds were within ranges of 10–18, 11–24, and 10–11 counts for Zn, Pb, and Cd, respectively. Fig. 1 illustrates the time scan and

Open Access Article. Published on 05 February 2026. Downloaded on 4/22/2026 12:07:22 PM. This article is licensed under a Creative Commons Attribution-NonCommercial 3.0 Unported Licence.

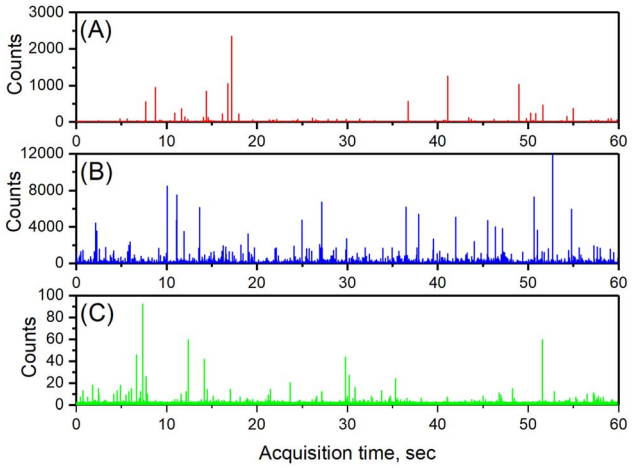

Fig. 1 An illustration of the time scan and signal of metal-containing nanoparticles (NPs) of Zn (A), Pb (B), and Cd (C) in the urban snow sample collected from Winnipeg on December 18, 2022, for Pb and Cd, and on April 7, 2023, for Zn.

signal in the urban snow sample collected on April 7, 2023, for Zn-containing NPs and January 19, 2023, for Cd-and Pb-containing NPs.

As shown in Fig. 2, in the snow samples, the most frequent equivalent diameters were 65.6 nm (range: 38.2–186 nm) for Zn-containing NPs (collected on April 7), and 72.0 nm (range: 52–180 nm) and 40 nm (range 26.0–55 nm) for Pb- and Cd-containing NPs (collected on December 18), respectively. The mass of Zn-, Pb-, and Cd-per containing NPs ranged from 0.2 to 31, 0.6 to 36.4, and 0.05 to 1.1 fg, respectively. Notably, the most frequent mass of Zn-, Pb-, and Cd-per containing NPs was 0.9, 4.7, and 0.18 fg, respectively.

Table 1 shows the particle concentration, average mass of the element per nanoparticle, and equivalent diameter of Zn-, Pb-, and Cd-containing NPs in snow samples collected from Winnipeg during the winter months of 2022 and 2023. Particle concentrations ranged from 2.7×10^5 to 2.0×10^7 particles/L for Zn-containing NPs and 2.9×10^5 to 2.5×10^7 particles/L for Pb-containing NPs. In the detected particles of Cd-containing NPs, the particle concentration varied from 6.1×10^5 to 3.5×10^6 particles/L. Average mass of the element per nanoparticle varied from 1.9 to 7.7, 5.0 to 12.0, and 0.27 to 0.4 fg for Zn-, Pb-, and Cd-containing NPs, respectively. LOD_{size} for Zn-, Pb-, and Cd-containing NPs ranged from 49.5 to 60.3 nm, 78.0 to 102.5 nm, and 28.9 to 30.0 nm, respectively. All $LOD_{(size)}$ values are presented in Table S2.

The snow samples collected from the downtown area showed higher particle concentrations for Zn-containing NPs throughout the winter and early spring than those collected on the UM campus, approximately 9 km from the downtown

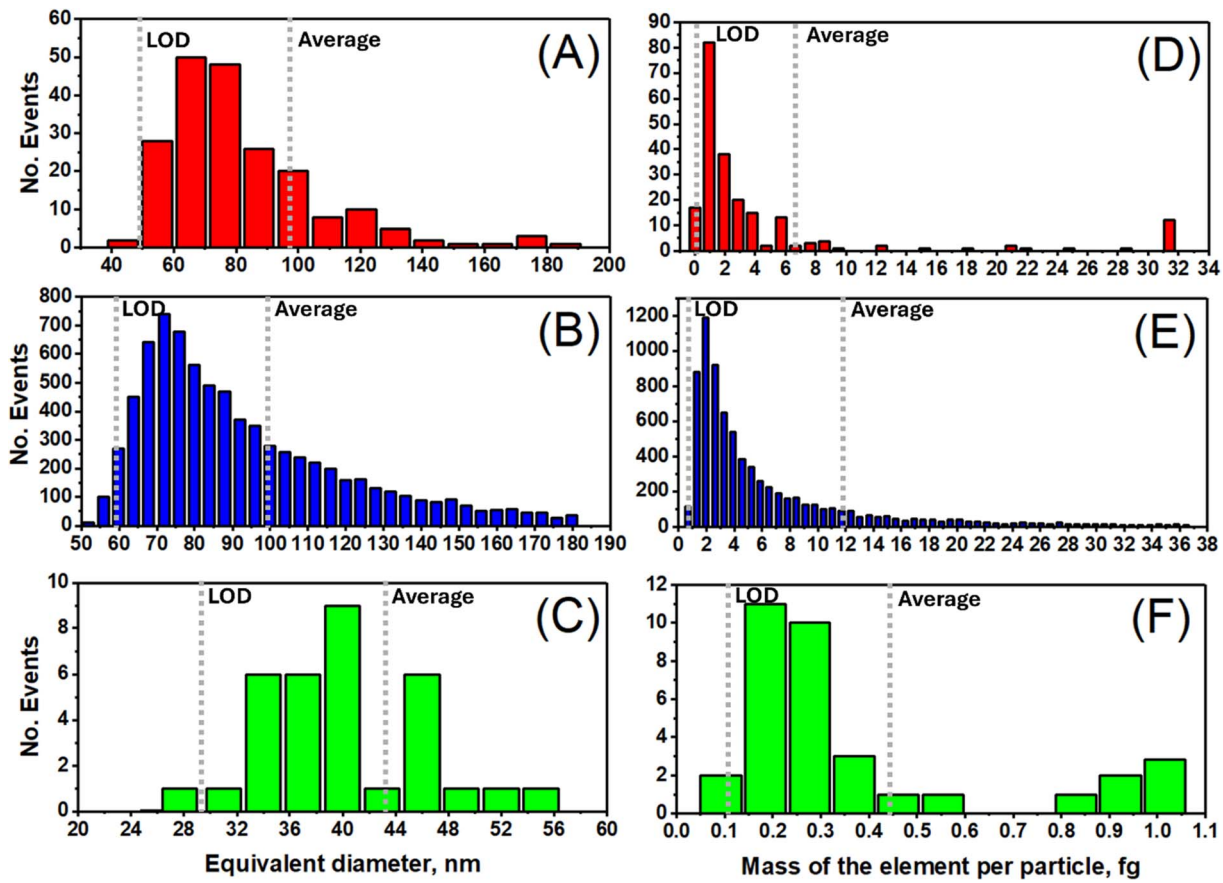

Fig. 2 Distribution patterns of the equivalent diameter (A–C) and mass of the element per particle (D–F) for Zn- (red), Pb- (blue), and Cd- (green) in snow collected from Winnipeg on December 18, 2022, for Pb and Cd, and April 7, 2023, for Zn.

© 2026 The Author(s). Published by the Royal Society of Chemistry

Open Access Article. Published on 05 February 2026. Downloaded on 4/22/2026 12:07:22 PM.
This article is licensed under a Creative Commons Attribution-NonCommercial 3.0 Unported Licence.

Table 1 The concentration, average mass of the element per nanoparticle, and average equivalent diameter of Zn-, Pb- and Cd-containing NPs in snow collected from an urban area (Winnipeg) in the winter/spring of 2022/2023

	Zn			Pb			Cd		
Sample ID	Particle concentration (particles/L)	$\tilde{x}$ mass per NP[f] (fg)	Average diameter (nm)	Particle concentration (particles/L)	$\tilde{x}$ mass per NP[f] (fg)	Average diameter (nm)	Particle concentration (particles/L)	$\tilde{x}$ mass per NP[f] (fg)	Average diameter (nm)
[a]Downtown Nov. 4, 2022	4.5×10^5	2.9 ± 2.6	85.1 ± 23.7	1.0×10^7	8.6 ± 26.2	92.9 ± 40.2	ND	ND	ND
[a]Downtown Dec. 18, 2022	9.0×10^5	2.0 ± 0.9	78.5 ± 13.4	2.5×10^7	12.0 ± 47.0	102.5 ± 45.3	3.5×10^6	0.4 ± 0.3	43.9 ± 10.2
[a]Downtown Jan. 19, 2023	3.0×10^6	11.6 ± 23.4	116 ± 57	2.3×10^7	8.7 ± 29.7	95.6 ± 37.6	6.1×10^5	0.4 ± 0.1	42.4 ± 6.0
[d]UM April 5, 2023	2.7×10^5	2.8 ± 2.2	84.6 ± 23.3	2.9×10^5	5.1 ± 10.8	81.8 ± 31.0	ND	ND	ND
[e]UM April 6, 2023	2.7×10^5	2.8 ± 2.2	84.6 ± 23.3	3.5×10^5	5.0 ± 12.2	79.5 ± 32.1	ND	ND	ND
[b]Downtown April 7, 2023	2.0×10^7	7.7 ± 20.6	98.7 ± 50.0	7.5×10^5	4.0 ± 6.0	77.9 ± 26.1	ND	ND	ND
[c]Downtown April 7, 2023	7.2×10^5	2.5 ± 1.3	84.7 ± 14.8	3.2×10^5	5.7 ± 17.7	82.1 ± 33.7	ND	ND	ND
[a]Downtown April 20, 2023	1.3×10^6	2.1 ± 1.5	79.5 ± 16.7	5.5×10^6	5.3 ± 11.4	84.4 ± 29.4	2.9×10^6	0.27 ± 0.01	38.4 ± 4.6

[a] Osborne village area (Winnipeg–Downtown). [b] Assiniboine river (Winnipeg–Downtown). [c] The Forks (Winnipeg–Downtown). [d] Gym area at the University of Manitoba (UM). [e] Chemistry department at the UM; ND – not detected. [f] The mass of the element per nanoparticle was indicated in the table heading as mass per NP.

© 2026 The Author(s). Published by the Royal Society of Chemistry

Open Access Article. Published on 05 February 2026. Downloaded on 4/22/2026 12:07:22 PM.
This article is licensed under a Creative Commons Attribution-NonCommercial 3.0 Unported Licence.

sampling area. Zn-containing NPs were more concentrated in the snow on January 19, 2022, April 7, 2023, and April 20, 2023, as particle concentrations were 3.0×10^6 particles/L, 2.0×10^7 particles/L, and 1.3×10^6 particles/L, respectively. The lower particle concentrations of 2.7×10^5 particles/L were measured at UM on April 5 and 6, respectively. On January 19 (Osborne Village) and April 7 (Assiniboine River), the snow samples contained the highest Zn mass per containing NPs was calculated as 11.6 and 7.7 fg, respectively. On January 19, the average mass of Zn per containing nanoparticle was 5.9-fold heavier compared to the particles measured on December 18. Most of the snow samples collected from November 4, 2022, to April 20, 2023, showed similar Zn-containing NPs equivalent diameter, averaging approximately 89 nm.

For Pb-containing NPs, higher particle concentrations were measured in winter, from November 4, 2022, to January 19, 2023, and April 20, 2023. The particle concentration in the snow samples collected in these months ranged from 5.5×10^6 to 2.5×10^7 particles/L. As observed for Zn-containing NPs, higher particle concentrations were measured in the downtown area than on the UM campus. The heavier mass of Pb per containing NP was measured on November 4, December 18, and January 19, with averages of 8.6, 12.0, and 8.7 fg, respectively. The average mass of Pb per containing nanoparticle from April 5 to April 20 was approximately 6.8 fg. Notably, the mass of Pb per containing nanoparticle on December 18 was 3-fold heavier than on April 7 (Assiniboine River). Larger average particle equivalent diameters of 92.9, 102.5, 95.6, and 84.4 nm were detected in the snow samples collected from downtown on November 4, December 18, January 19, and April 20, respectively. In contrast, average equivalent diameters of 81.8, 79.5, 77.9, and 82.1 nm were evaluated on April 5, 6, and 7 (Assiniboine River and The Forks), respectively.

Cd-containing NPs were detected on December 18, January 19, and April 20, 2023, with concentrations of 3.5×10^6, 6.1×10^5, and 2.9×10^6 particles/L, respectively. Among the three months, December 18 had the highest number of particles in the snow samples, 5.7 and 1.2-fold higher than particles from January 19 and April 20, respectively.

The mass concentrations of Zn-, Pb-, and Cd-containing NPs exhibited variability across different months, as illustrated in Fig. 3. Specifically, the mass concentration of Zn-containing NPs ranged from 0.7 to 149 ng L^{-1}, with the maximum value of 149 ng L^{-1} recorded in snow samples collected from the Assiniboine River area on April 7, 2023. The mass concentrations of Pb- and Cd-containing NPs varied from 1.5 to 296 ng L^{-1} and 0.2 to 1.6 ng L^{-1}, respectively. The highest concentrations were observed in the Assiniboine River area for

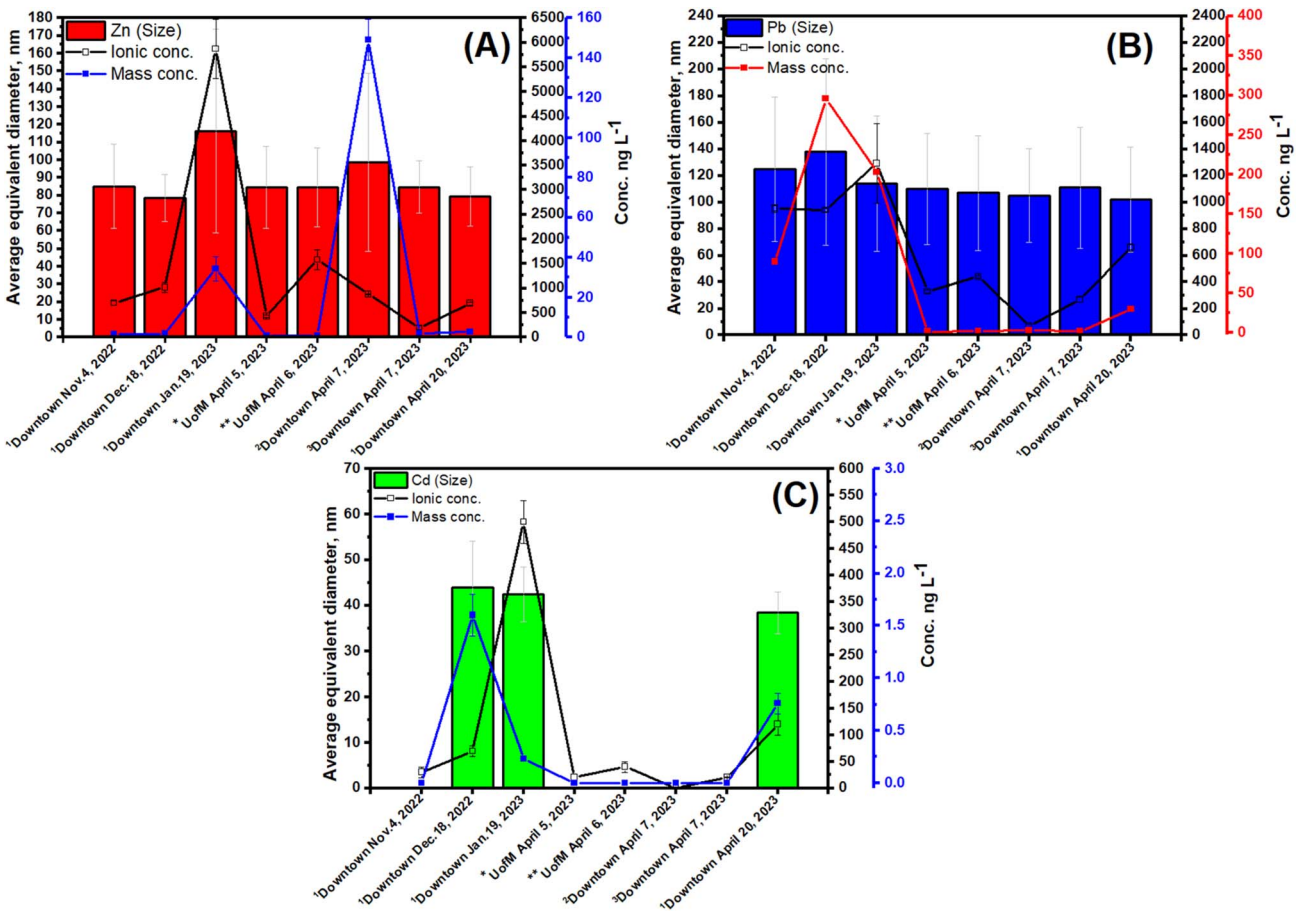

Fig. 3 Average equivalent diameter, total concentration, and mass concentration distribution of the metal-containing nanoparticles (NPs) (A) Zn-, (B) Pb-, and (C) Cd-containing NPs of the snow collected in Winnipeg during winter/spring of 2022–2023.

© 2026 The Author(s). Published by the Royal Society of Chemistry

Open Access Article. Published on 05 February 2026. Downloaded on 4/22/2026 12:07:22 PM. This article is licensed under a Creative Commons Attribution-NonCommercial 3.0 Unported Licence.

Zn-containing NPs and in the Downtown area for Pb- and Cd-containing NPs on December 18, 2022. Concurrently, total concentrations of Zn, Pb, and Cd were determined in snow samples collected from November 2022 to April 2023 to assess the proportion of NPs in the samples. Consequently, the total concentrations ranged from 0.2 to 5.9 μg L^{-1} for Zn, 0.1 to 1.3 μg L^{-1} for Pb, and 0.02 to 0.50 μg L^{-1} for Cd. The percentage of NPs within the total metal concentrations varied from 0.05 to 17% for Zn, 0.2 to 31.5% for Pb, and 0.05 to 2.2% for Cd. Complete data on concentrations and percentages are provided in Table S3.

A different trend in the mass and total concentration of Zn-, Pb- and Cd-containing NPs was observed throughout the winter and early spring. During the early cold months (November and December 2022, Downtown area), the mass concentrations of Zn-, Pb-, and Cd-containing NPs ranged from 0.7 to 149 ng L^{-1}, 1.5 to 296 ng L^{-1}, and 0.2 to 1.6 ng L^{-1}, respectively. Subsequently, the maximum mass concentration of NPs was observed on the Assiniboine River area on April 7, 2023, and December 18, 2022 (Osborne Village), with concentrations of 149 ng L^{-1} for Zn-containing NPs, 296 ng L^{-1} for Pb-containing NPs and 1.6 ng L^{-1} for Cd-containing NPs. In early spring, the mass concentration of Pb- and Cd-containing NPs decreased compared to December 18, ranging from 1.5 to 29.0 ng L^{-1} and 0.2 to 0.8 ng L^{-1}, respectively. From November to January 2023, the mass concentration of Pb-containing NPs accounted for 0.2–31.5% and 0.4–4.2% from April 5 to April 20, 2023, compared to the total concentration. For Cd-containing NPs, the mass concentration accounted for 0.05–2.2% from November to January 2023 and 0–0.6% from April 5 to April 20, 2023, compared to the total concentration (values available in Table S3).

Contrary to Pb- and Cd-containing NPs, Zn-containing NPs reached their maximum mass concentration on April 7, 2023 (Assiniboine River), with 149 ng L^{-1}. Additionally, on January 19, Zn-containing NPs mass concentration was also elevated (34.4 ng L^{-1}), compared to early winter and some days in the spring season. On April 7 (Assiniboine River), the mass concentration was 201, 84, and 55-fold higher than the samples collected on April 5 (UM), April 7 (The Forks), and April 20 (Downtown area-Osborne Village), respectively.

Although there is a lack of literature studies on Zn-, Pb- and Cd-containing NPs in snow samples, two recent studies have characterized Ti-, Ce- and Ag-NPs in precipitation samples from several major cities in the World, as well Al-NPs in two snowstorms in Colorado, USA.[25,26] Ti-, Ce- and Ag-NPs particle

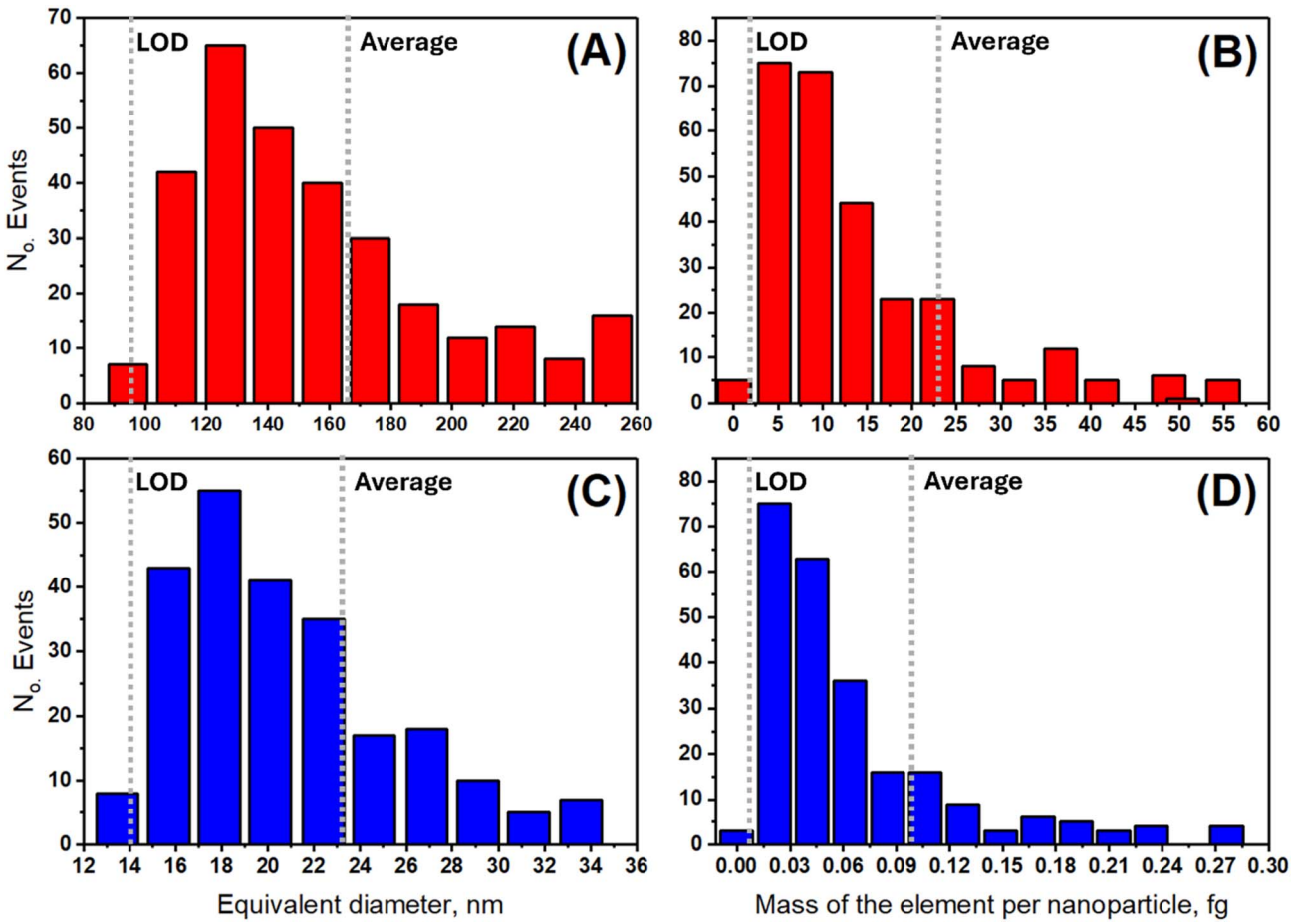

Fig. 4 Distribution patterns of the equivalent diameter (A and C) and mass of the element per particle (B and D) for Zn- (red) and Pb- (blue) in a snowpit collected from Müller Ice Cap at 20 cm depth.

Open Access Article. Published on 05 February 2026. Downloaded on 4/22/2026 12:07:22 PM. This article is licensed under a Creative Commons Attribution-NonCommercial 3.0 Unported Licence.

concentrations were often within the range of 10^7–10^{10} NP/L, and 10^8–10^{11} particles/L for Al-NPs. The snow concentrations of NPs in our study for Zn-, Pb-, and Cd-containing NPs ranged are lower than those concentrations.

3.2. Zn- and Pb-containing NPs in the Arctic snowpit

Only Zn- and Pb-containing NPs were detectable in the Müller Ice Cap snowpit; Cd-containing NPs could not be detected due to minimal pulse signals lower than detection threshold values. The detection thresholds were determined to be 10–15 and 10–11 counts for Zn and Pb, respectively. The raw data from a depth of 20 cm is illustrated in Fig. S2, where the signal distribution (NP pulses) is plotted against the acquisition time (60 s).

Further analysis of each analyte pulse signal revealed detailed information on the equivalent diameter, the mass of the element per nanoparticle, and the percentage mass distribution of Zn- and Pb-containing NPs, measured and calculated in the snowpit. In Fig. 4, the equivalent diameter distribution is illustrated at a depth of 20 cm.

The equivalent diameter distribution of Zn-containing NPs in the snowpit sample at a depth of 20 cm ranged from 94.5 to 252 nm, with 126 nm being the most frequently measured equivalent diameter. The mass of Zn per containing NPs distribution ranged from approximately 0.58 to 59 fg, with 4.6 fg being the most frequently observed mass of the element per nanoparticle. Equivalent diameters ranging from 13.5 to 33.6 nm were measured for Pb-containing NPs, with 17.9 nm being the most frequent equivalent diameter, and the observed mass of Pb per containing nanoparticle ranged from approximately 1.1 to 234 ag. The highest detectable frequency corresponded to a mass of Pb per containing nanoparticle of 21.2 ag.

The particle concentration, average mass of the element per nanoparticle, and equivalent diameter of Zn- and Pb-containing NPs in the Müller Ice Cap snowpit samples from depths of 10 to 60 cm are presented in Table 2. For Zn-containing NPs, the particle concentration ranged from 2.0×10^6 to 3.2×10^6 particles/L, whereas Pb-containing NPs particle concentration was measured from 4.6×10^6 to 2.8×10^7 particles/L. Average masses varied from 5.0 to 144.7 fg and 102.8 to 138.3 ag for Zn- and Pb-containing NPs, respectively. The average equivalent diameters were calculated based on the mass of the element per nanoparticle values, ranging from 94.0 to 298.7 nm for Zn and 23.4 to 24.6 nm for Pb-containing NPs. The $LOD_{(size)}$ for Zn- and Pb-containing NPs ranged from 69.5 to 167.8 nm, and 13.2 to 14.2 nm, respectively, as presented in Table S4.

Higher particle concentrations of Zn-containing NPs were observed at depths ranging from 20 to 50 cm, with concentrations varying from 2.0 to 3.2×10^6 particles/L, and the highest concentration was measured at 20 cm. The lowest concentration was observed at the deepest depth (60 cm; 1.7×10^6 particles/L). The larger Zn-containing NPs equivalent diameters were 166.8, 298.7, and 114.3 nm at snowpits of 20, 30, and 40 cm, respectively. In addition, average equivalent diameters of 112.4, 96.3, and 94.0 nm were observed in snowpits of 10, 50, and 60 cm, respectively. The average equivalent diameters derived from the snowpit at the Müller Ice Cap were larger than those obtained from snow samples within the urban area. The equivalent diameter of Zn-containing NPs measured in Winnipeg ranged from 78.5 to 116.4 nm, whereas at the Müller Ice Cap, the equivalent diameters ranged from 94.0 to 298.7 nm. The average equivalent diameter from the Müller Ice Cap snowpit (147 nm) was approximately 1.65-fold larger than the average equivalent diameter measured in Winnipeg, which was 89.0 nm.

For Pb-containing NPs, snowpits at 20, 30, 40, and 60 cm accumulated more particles than the 10 and 50 cm snowpit samples. Particle concentrations from 1.6 to 2.8×10^7 particles/L were measured from 20, 30, 40, and 60 cm, whereas 4.6 to 6.5×10^6 particles/L were detected in the snowpits at 10 and 50 cm. For comparison, the particle concentration of Pb-containing NPs at 30 cm was 3.6-fold higher than that at 50 cm. Throughout the investigated depths from 10 to 60 cm, the average mass of Pb per containing nanoparticle and the average equivalent diameter were similar, ranging from 103 to 108 ag and 23.4 to 24.6 nm, respectively. The equivalent diameters of Pb-containing NPs in the Müller Ice Cap were 4.8-fold smaller compared to those in urban snow, contrary to the observations of Zn-containing NPs, as presented in Fig. 5.

Mass concentrations of Zn- and Pb-containing NPs in the snowpit samples from 10 to 60 cm were measured, as illustrated in Fig. 3. For Zn-containing NPs, the mass concentration ranged from 10.0 to 296.7 ng L^{-1}, of which, at 30 cm, the maximum mass

Table 2 Particle concentration, mass of the element per nanoparticle and average equivalent diameter of Zn, Pb and Cd-containing NPs in the snowpit collected from the Müller Ice Cap

	Zn			Pb		
Snowpit depth (cm)	Particle concentration (particles/L)	$\tilde{x}$ mass per NP[a] (fg)	Average diameter (nm)	Particle concentration (particles/L)	$\tilde{x}$ mass per NP[a] (ag)	Average diameter (nm)
10	2.2×10^6	7.8 ± 17.6	112.4 ± 38.8	4.6×10^6	118.8 ± 200.5	23.6 ± 8.7
20	3.2×10^6	23.0 ± 34.5	166.8 ± 50.2	2.8×10^7	102.8 ± 144.8	23.4 ± 7.2
30	2.0×10^6	144.7 ± 290.2	298.7 ± 101.4	2.3×10^7	115.0 ± 245.6	23.5 ± 8.0
40	2.9×10^6	8.0 ± 13.4	114.3 ± 39.1	1.6×10^7	125.1 ± 186.0	24.6 ± 8.2
50	2.9×10^6	4.9 ± 9.8	96.3 ± 32.9	6.5×10^6	138.3 ± 313.6	23.8 ± 9.9
60	1.7×10^6	5.7 ± 19.3	94.0 ± 40.0	1.7×10^7	116.1 ± 216.2	23.5 ± 8.5

[a] The mass of the element per nanoparticle was indicated in the table heading as mass per NP.

 © 2026 The Author(s). Published by the Royal Society of Chemistry

Open Access Article. Published on 05 February 2026. Downloaded on 4/22/2026 12:07:22 PM.
This article is licensed under a Creative Commons Attribution-NonCommercial 3.0 Unported Licence.

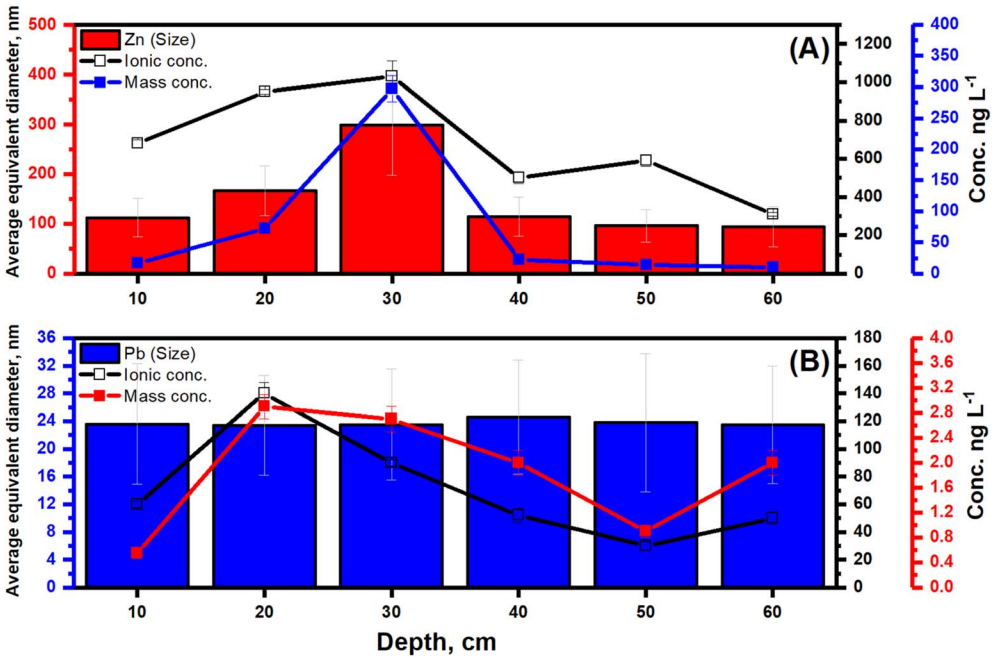

Fig. 5 Average equivalent diameter, total concentration and mass concentration distribution of the metal-containing nanoparticles (NPs) (A) Zn and (B) Pb in the snowpit depth from Müller Ice Cap.

concentration was measured as 296.7 ng L^{-1}. A lower mass concentration of Pb-containing NPs was observed in comparison to Zn-containing NPs, ranging from 0.5 to 2.9 ng L^{-1}, with the maximum concentration measured at 20 cm. The total concentrations of Zn and Pb were also measured in the snowpit samples at depths ranging from 10 to 60 cm to calculate the NP percentage. Hence, the total concentration of Zn and Pb ranged from 0.3–1.0 μg L^{-1} and 30.0–140 ng L^{-1}, respectively, whereas the NP percentage accounted for 2.4–28.8% for Zn and 0.9–3.9% for Pb. The complete concentration and percentage data are presented in Table S5.

The observed trend in mass concentration for Zn and Pb-containing NPs indicates higher concentrations between 20 to 30 cm, with lower concentrations at 10 cm and the deepest section of the pit (50 to 60 cm). Specifically, within the range of 20 to 30 cm, the mass concentration of Zn- and Pb-containing NPs ranged from approximately 73 to 297 ng L^{-1} and 2.9 to 2.7 ng L^{-1}, respectively. At a depth of 10 cm, the concentrations were measured at 16.9 ng L^{-1} for Zn-containing NPs and 0.5 ng L^{-1} for Pb-containing NPs. Conversely, at 60 cm, concentrations of 10 and 1.9 ng L^{-1} were detected for Zn- and Pb-containing NPs, respectively. The total concentration of Zn-containing NPs follows a similar trend to the mass concentration. For instance, at 30 cm, the total concentration of Zn was approximately 1.0 μg L^{-1}, decreasing from 0.5 to 0.3 μg L^{-1} at depths from 40 to 60 cm.

The mass concentration of Pb-containing NPs exhibited variation across different depths. In the upper part (between 10 and 20 cm), it increased from 0.5 to 2.9 ng L^{-1} (approximately 5.8-fold) and remained constant until 30 cm. Compared to the mass concentration at 20 cm, it decreased by 3.2-fold at 50 cm and 1.5-fold at 60 cm. The total concentration revealed comparable variability to the mass concentration. An increase from 60 to 140 ng L^{-1} was observed from 10 to 20 cm, respectively, and decreased from 30 to 60 cm, with values ranging from 90 to 30 ng L^{-1}.

4. Discussion

4.1. Metal-containing nanoparticles source and transport in the atmosphere

In Winnipeg, the average particle concentration of Zn-, Pb-, and Cd-containing NPs is 3.3, 3.3, and 2.3 × 10^6 particles/L, respectively. In an urban area, incidental nanoparticles (INPs), a by-product of vehicle exhaust and non-exhaust emissions, generate a significant number of nanoparticles, with concentrations ranging from 10^7 to 10^9 particles per cm of air in the tailpipe aerosol.[27] These nanoparticles vary in size, physical properties, and chemical composition. For instance, it contains particles with diameters ranging from 10 nm to several hundred nanometers, with a mean particle size typically between 30–100 nm.[27]

The particle concentration of Zn-containing NPs in the urban environment, compared to Pb- and Cd-containing NPs is associated with exhaust emissions, primarily vehicle-related environmental emissions.[6] Studies have indicated that non-exhaust traffic sources, including tire dust, also release ZnO as it is added as an activator during the vulcanization process, compromising 0.4 to 4.3% of the resulting tire material.[6,8] On the other hand, the release of Pb and Cd into the atmosphere may be attributed to exhaust and non-exhaust-related activities, such as burning diesel and gasoline, tires, brake/road dust, paint, and abraded asphalt.[8] For instance, it is estimated that brake wear contributes between 16 and 55%, and tire dust

Open Access Article. Published on 05 February 2026. Downloaded on 4/22/2026 12:07:22 PM. This article is licensed under a Creative Commons Attribution-NonCommercial 3.0 Unported Licence.

contributes between 5 and 30% to re-suspended road dust.[8] Even though Zn-containing NPs are extensively released to the atmosphere by incidental and industrial activities, our study revealed that the particle concentration of Pb-containing NPs was higher in comparison to the Zn- and Cd-containing NPs in the urban environment. Over the months, the average mass concentration for Pb-containing NPs was 53.1 ng L^{-1}, compared to 24.1 and 0.9 ng L^{-1} for Zn- and Cd-containing NPs, respectively.

In the Arctic snowpit, the average particle concentration for Zn- and Pb-containing NPs was notably 1.6-fold lower and 2.1-fold higher than in the urban snow, respectively. Despite the unexpected presence of Zn- and Pb-containing NPs in the Arctic compared to urban environments, their occurrence may be associated to PM transport originating from local Arctic emissions, including transportation activities such as shipping, as well as industrial processes related to oil and gas extraction, metal smelting, and mineral extraction.[11] The Arctic haze is a potential source of fine PM during winter and early spring in the High Arctic.[11] Additionally, atmospheric chemical reactions can influence the behavior of NPs in air pollutants under unique Arctic conditions. Factors such as extreme cold, dry air, and reduced solar radiation during winter months can affect the agglomeration, aggregation, or dissolution of NPs.

Notable differences were observed when comparing average equivalent diameters for Zn- and Pb-containing NPs in the urban and Arctic environments. The average equivalent diameter of Zn- and Pb-containing NPs in the Müller Ice Cap snowpit ranged from 94 to 298.7 nm and 23.4 to 24.6 nm, respectively. In contrast, the average equivalent diameters of Zn-containing NPs ranged from 78.5 to 116 nm, and those of Pb-containing NPs ranged from 105 to 138 nm, as measured in the urban area. This enormous contrasting average equivalent diameters detected for Zn-containing NPs in the urban and Arctic environments could be associated with atmospheric reactions arising from organic and inorganic compounds, leading to greater dissolution, agglomeration, or aggregation, as occurs to ZnO in an aquatic medium.[28,29] Photochemical processes related to the exposure of Zn-NPs under solar radiation could also enhance or reduce the agglomeration/dissolution of the particles.[30,31] In contrast with Zn-NPs, the transformation of the Pb- and Cd-NPs in the atmosphere is, to the best of our knowledge, unknown.[2,6,32]

As stated, the presence of metal-containing NPs in urban environment is likely associated with traffic and industrial activities. Conversely, identifying potential sources of these particles in the High Arctic poses a challenge due to limited information and system complexity. The detection of multi-metal particles using time-of-flight mass spectrometry (TOF MS) could be used to discriminate between natural nanoparticles (NNPs) and engineered nanoparticles (ENPs) in the snow samples. Unfortunately, this discrimination is not feasible using quadrupole mass spectrometry (QMS).

LOD_{size} values are comparable with those achieved by a recent sp-ICP-ToF-MS study.[33] For instance, the LOD_{size} for Zn, Pb, and Cd reported by the sp-ICP-ToF-MS study was 54.2, 15.7, and 22.1 nm, respectively; whereas in our study, the lowest LOD_{size} achieved for Zn, Pb, and Cd was 49.5, 13.2, and 28.9 nm, respectively.

It is worth noting that the residence time of the metallic NPs was different in the snow collected in the urban and Arctic areas. In the urban area, the snow was freshly collected as the snowflakes were deposited on the ground. In contrast, samples were collected from the Müller Ice Cap by digging a snowpit in May 2023. Depending on the depth, the NPs were in contact with the snow for a minimum of 2 to 3 months before the sample was collected. This factor could also contribute to the equivalent diameter and mass of the element per nanoparticle differences observed for Zn- and Pb-NPs. Furthermore, we acknowledge that transport (*e.g.*, refreezing) and processing (*e.g.*, melting prior to lab analysis) of the remote Müller Ice Cap samples may also modify the characteristics of the NPs *via* processes such as aggregation and agglomeration.

Additionally, it is noteworthy that the distribution of equivalent diameters generally decreases progressively with an increase in baseline intensity, thereby complicating the distinction between particle events and dissolved species. Nevertheless, the baseline varies among our samples, producing, in most cases, a half-size distribution. Accordingly, the results presented should be regarded as semi-quantitative or qualitative.

The use of sp-ICPMS, combined with TEM-EDX, would facilitate the verification of the size distribution of metal-containing nanoparticles. However, due to the low particle concentration in snow samples, TEM was unable to detect individual Zn, Pb, and Cd particles.

4.2. Identification of potential source regions

A diagram plotting Pb^{206}/Pb^{207} against Pb^{208}/Pb^{207}, obtained *via* ICP-MS/MS, was used to identify potential source regions of atmospheric Pb influencing both urban and High Arctic environments. The measured data were compared to the literature signatures.[34–37] As illustrated in Fig. 6, distinct sources of Pb were identified in Winnipeg and the Müller Ice Cap snow. This observation aligns with expectations, considering the varying air masses that transport pollutants to different regions of Canada. In the urban area, the Pb isotope signatures indicate a substantial contribution from Canadian aerosols, likely coming from urban traffic-related sources, predominantly exhaust and non-exhaust processes, including fossil fuel combustion and tire dust.[38] These signatures support the hypothesis outlined previously, suggesting that the snow matrix subsequently captures local atmospheric emissions. Notably, two snow samples collected in Winnipeg—one from the Assiniboine River Downtown area on April 7, 2023, and another from the Chemistry Department at the University of Manitoba on April 6, 2023—revealed anthropogenic aerosols originating from the United States, signifying a mixture of sources during this specific spring period. Although atmospheric Pb emissions in North America have decreased due to the prohibition of leaded gasoline in the late 20th century, significant sources in Canada and the United States continue from processes

 © 2026 The Author(s). Published by the Royal Society of Chemistry

Open Access Article. Published on 05 February 2026. Downloaded on 4/22/2026 12:07:22 PM.
This article is licensed under a Creative Commons Attribution-NonCommercial 3.0 Unported Licence.

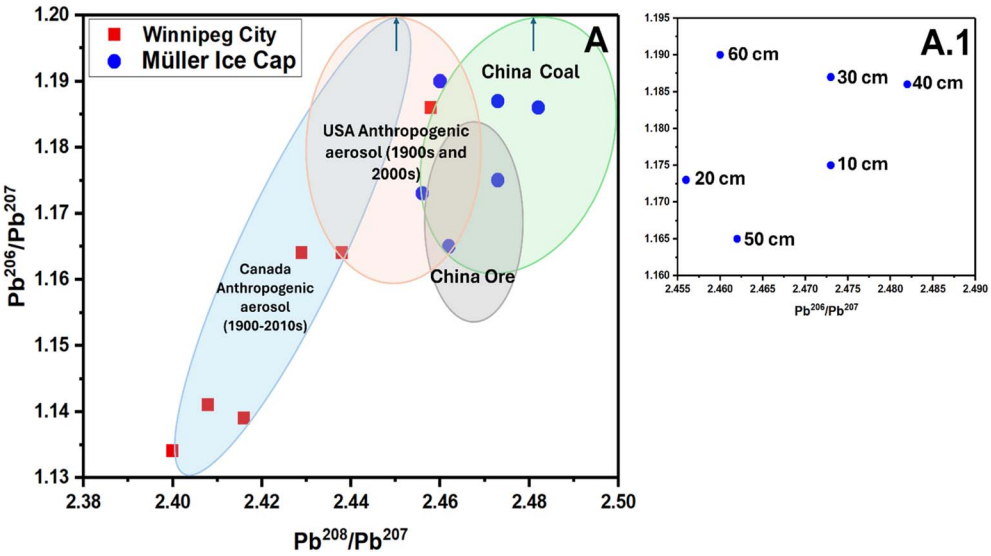

Fig. 6 Diagram of Pb^{206} Pb^{207} and Pb^{208} Pb^{207} ratios from the snow collected in Winnipeg and the snowpit from the Müller Ice Cap. (A) Based on the Pb isotopic values from Chinese ores (Pb^{206} Pb^{207}: 1.160 ± 0.015 and Pb^{208} Pb^{207}: 2.468 ± 0.011);[39] Chinese coals (Pb^{206} Pb^{207}: 1.190 ± 0.030 and Pb^{208} Pb^{207}: 2.483 ± 0.034);[39] United States anthropogenic aerosols (Pb^{206} Pb^{207}: 1.1588–1.2314 and Pb^{208} Pb^{207}: 2.4261–2.4703);[37] and Canadian anthropogenic aerosols (Pb^{206} Pb^{207}: 1.0943–1.206 and Pb^{208} Pb^{207}: 2.404–2.445).[34,36,37] (A.1) Detailed Pb^{206} Pb^{207} isotopic values based on the Müller Ice Cap snowpit samples at different depths.

originating from metalworking, aviation fuel, and coal combustion.[38]

In the High Arctic, Pb isotopic signature indicate aerosol originating from various sources, predominantly characterized by smelting and other industrial activities, as well as emissions from China.[35] The long-range transport of Pb, and potentially Pb-containing NPs, during spring results from Arctic haze, which is caused by substantial pollutant inputs from Asia and Eurasia into the Arctic air mass.[11] Complementing the analysis of Pb isotope ratio in the Müller Ice Cap snowpit, recent Greenland snow samples have identified increased Pb isotope signatures influenced by pollutant aerosols originating from China.[35] This evidence shows the long-range transport of aerosols from Asia to the High Arctic regions. Although the deposition levels of Pb and other emerging pollutants, including metallic NPs, remain relatively low, this study confirms that remote Arctic locations continue to accumulate anthropogenic substances from distant regions.

Although the isotopic ratio analysis was conducted based on the ionic content in the surface and snowpit samples, it can indicate potential source regions of metal-containing nanoparticles, including Zn, Pb, and Cd. Additionally, it is advantageous to differentiate pollution sources between urban and distant areas, and to consider how long-distance transportation, particularly in spring, may influence the composition of air masses that ultimately deposit onto the surface through wet deposition.

5. Conclusion

The use of spICP-MS is shown to be a valuable analytical technique for characterizing Zn-, Pb-, and Cd-containing NPs in snow samples from urban and High Arctic areas, where the mass concentrations ranged from μg L^{-1} to ng L^{-1}. The urban and Arctic areas exhibit distinct average equivalent diameters, suggesting different environmental transformations for these NPs. In the urban environment, a higher release of Pb-containing NPs was observed in the winter than in the spring season. In contrast, no such seasonal difference was noted for Zn- and Cd-containing NPs. Additionally, the mass of the element per nanoparticle of the evaluated NPs was found to be heavier on January 19, 2023, in Winnipeg and in the samples taken at the depth of 30 cm in the Müller Ice Cap.

Using the single-particle mode may facilitate monitoring of metal-containing nanoparticles released into the atmosphere from both anthropogenic and natural sources. However, predicting NP species in urban and Arctic environments remains challenging due to their high dynamism, driven by significant anthropogenic, natural, and incidental contributions. Further studies are necessary to comprehend the transformation of Zn-, Pb-, and Cd-containing NPs in the atmosphere, considering aspects such as size, species, dissolution, and agglomeration, as previous studies on the fate and reactions of NPs in the environment have predominantly focused on aquatic systems.

Given the importance of identifying anthropogenic sources and comprehending the transport and distribution of NPs in the environment, the analysis of Pb isotopic ratios *via* ICP-MS/MS suggests a local release of aerosols within the urban environment, primarily associated with traffic and industrial activities, as well as long-range atmospheric transport to the High Arctic associated with anthropogenic aerosols originating from Asia and North America. Although the concentrations of NPs in the remote Arctic snowpit remain relatively low, their presence highlights their ubiquitousness in the global environment.

© 2026 The Author(s). Published by the Royal Society of Chemistry

Open Access Article. Published on 05 February 2026. Downloaded on 4/22/2026 12:07:22 PM. This article is licensed under a Creative Commons Attribution-NonCommercial 3.0 Unported Licence.

Further investigations are warranted to understand better global transport and transformation of these metal-containing NPs and their potential risks to ecological and human health, particularly in remote and pristine areas.

Conflicts of interest

There are no conflicts to declare.

Data availability

Data are available through the Canadian Watershed Information Network (CanWIN) data repository at https://doi.org/10.34992/emwm-4426.

Supplementary information (SI) is available. See DOI: https://doi.org/10.1039/d5va00258c.

Acknowledgements

This study was funded by the Canada Excellence Research Chairs (D. D.-J.) and Canada Research Chairs (F. W.) programs and the Natural Sciences and Engineering Research Council of Canada (F. W.). The authors acknowledge the contribution of Debbie Armstrong from the Centre for Earth Observation Science (University of Manitoba) for the assistance with ICP-MS analysis.

References

1 M. Ajdary, M. A. Moosavi, M. Rahmati, M. Falahati, M. Mahboubi, A. Mandegary, S. Jangjoo, R. Mohammadinejad and R. S. Varma, *Nanomaterials*, 2018, **8**, 634.
2 A. Rabajczyk, M. Zielecka, R. Porowski and P. K. Hopke, *Environ. Sci.: Nano*, 2020, **7**, 3233–3254.
3 Z. Liu, S. Ying, Y. Jiang, H. Takeuchi and Y. Huang, *Rev. Environ. Contam. Toxicol.*, 2023, **261**, 4–29.
4 S. Sonwani, S. Madaan, J. Arora, S. Suryanarayan, D. Rangra, N. Mongia, T. Vats and P. Saxena, *Front. Sustain. Cities.*, 2021, **3**, 1–20.
5 M. F. Hochella, D. W. Mogk, J. Ranville, I. C. Allen, G. W. Luther, L. C. Marr, B. P. McGrail, M. Murayama, N. P. Qafoku, K. M. Rosso, N. Sahai, P. A. Schroeder, P. Vikesland, P. Westerhoff and Y. Yang, *Science*, 2019, **363**, 1–10.
6 P. Sanderson, J. M. Delgado-Saborit and R. M. Harrison, *Atmos. Environ.*, 2014, **94**, 353–365.
7 K. Adachi and Y. Tainosho, *Environ. Int.*, 2004, **30**, 1009–1017.
8 S. Wagner, C. W. Funk, K. Müller and D. J. Raithel, *Sci. Total Environ.*, 2024, **926**, 171694.
9 N. Kumar, G. R. Palmer, V. Shah and V. K. Walker, *PLoS One*, 2014, **9**, 1–12.
10 N. Kumar, V. Shah and V. K. Walker, *J. Hazard. Mater.*, 2011, **190**, 816–822.
11 J. Schmale, S. R. Arnold, K. S. Law, T. Thorp, S. Anenberg, W. R. Simpson, J. Mao and K. A. Pratt, *Earths Future*, 2018, **6**, 1385–1412.
12 Y. Nazarenko, S. Fournier, U. Kurien, R. B. Rangel-Alvarado, O. Nepotchatykh, P. Seers and P. A. Ariya, *Environ. Pollut.*, 2017, **223**, 665–675.
13 H. E. Pace, N. J. Rogers, C. Jarolimek, V. A. Coleman, E. P. Gray, C. P. Higgins and J. F. Ranville, *Environ. Sci. Technol.*, 2012, **46**, 12272–12280.
14 A. K. Venkatesan, B. T. Rodríguez, A. R. Marcotte, X. Bi, J. Schoepf, J. F. Ranville, P. Herckes and P. Westerhoff, *Environ. Sci.*, 2018, **4**, 1923–1932.
15 S. Baur, T. Reemtsma, H. J. Stärk and S. Wagner, *Chemosphere*, 2020, **246**, 125765.
16 D. M. Schwertfeger, J. R. Velicogna, A. H. Jesmer, R. P. Scroggins and J. I. Princz, *Anal. Chem.*, 2016, **88**, 9908–9914.
17 R. Gonzalez de Vega, T. E. Lockwood, X. Xu, C. Gonzalez de Vega, J. Scholz, M. Horstmann, P. A. Doble and D. Clases, *Anal. Bioanal. Chem.*, 2022, **414**, 5671–5681.
18 I. Jreije, M. Hadioui and K. J. Wilkinson, *Talanta*, 2022, **238**, 123060.
19 G. Moreno-Martín, B. Gómez-Gómez, M. E. León-González and Y. Madrid, *Talanta*, 2022, **238**, 123033.
20 F. Laborda, A. C. Gimenez-Ingalaturre, E. Bolea and J. R. Castillo, *Spectrochim. Acta, Part B*, 2019, **159**, 105654.
21 J. Vidmar, L. Hässmann and K. Loeschner, *J. Agric. Food Chem.*, 2021, **69**, 9979–9990.
22 D. Mozhayeva and C. Engelhard, *J. Anal. At. Spectrom.*, 2019, **34**, 1571–1580.
23 U.S. Environmental Protection Agency, *Method 1669: Sampling Ambient Water for Trace Metals at EPA Water Quality Criteria Levels*, Washington, D.C., 1996.
24 T. E. Lockwood, R. Gonzalez De Vega and D. Clases, *J. Anal. At. Spectrom.*, 2021, **36**, 2536–2544.
25 A. Azimzada, I. Jreije, M. Hadioui, P. Shaw, J. M. Farner and K. J. Wilkinson, *Environ. Sci. Technol.*, 2021, **55**, 9836–9844.
26 A. J. Goodman, A. Gundlach-Graham, S. G. Bevers and J. F. Ranville, *Environ. Sci.: Nano*, 2022, **9**, 2638–2652.
27 T. Rönkkö and H. Timonen, *J. Alzheimer's Dis.*, 2019, **72**, 15–28.
28 S. W. Bian, I. A. Mudunkotuwa, T. Rupasinghe and V. H. Grassian, *Langmuir*, 2011, **27**, 6059–6068.
29 Y. Zhang, Y. Chen, P. Westerhoff and J. Crittenden, *Water Res.*, 2009, **43**, 4249–4257.
30 L. Zhang, M. Jeem, K. Okamoto and S. Watanabe, *Sci. Rep.*, 2018, **8**, 1–13.
31 A. El Golli, S. Contreras and C. Dridi, *Sci. Rep.*, 2023, **13**, 20809.
32 H. Zhang, B. Chen and J. F. Banfield, *J. Phys. Chem. C*, 2010, **114**, 14876–14884.
33 M. Barabash, H.-E. Ahabchane, M. Hadioui and K. J. Wilkinson, *Environ. Sci.: Nano*, 2025, **12**, 4994–5007.
34 T. Akerman, G. Spiers, P. Beckett, J. Anderson and F. Caron, *Water, Air, Soil Pollut.*, 2021, **232**, 1–17.

© 2026 The Author(s). Published by the Royal Society of Chemistry

Open Access Article. Published on 05 February 2026. Downloaded on 4/22/2026 12:07:22 PM.
This article is licensed under a Creative Commons Attribution-NonCommercial 3.0 Unported Licence.

35 B. G. Koffman, P. Saylor, R. Zhong, L. Sethares, M. F. Yoder, L. Hanschka, T. Methven, Y. Cai, L. Bolge, J. Longman, S. L. Goldstein and E. C. Osterberg, *Environ. Sci. Technol.*, 2022, **56**, 13107–13118.
36 M. Bagur and D. Widory, *Atmos. Res.*, 2020, **235**, 104794.
37 A. Bollhofer and K. J. R. Rosman, *Geochim. Cosmochim. Acta*, 2002, **66**, 1375–1386.
38 J. Chételat, B. Cousens, C. E. Hebert, T. S. Jung, L. Mundy, P. J. Thomas and S. Zhang, *Environ. Pollut.*, 2022, **302**, 119074.
39 B. G. Koffman, P. Saylor, R. Zhong, L. Sethares, M. F. Yoder, L. Hanschka, T. Methven, Y. Cai, L. Bolge, J. Longman, S. L. Goldstein and E. C. Osterberg, *Environ. Sci. Technol.*, 2022, **56**, 13107–13118.